Journal of Photochemistry and Photobiology A: Chemistry 202 (2009) 107–114

Contents lists available at ScienceDirect

Journal of Photochemistry and Photobiology A: Chemistry

journal homepage: www.elsevier.com/locate/jphotochem

The photoelectrochemical performances of Sb-doped $AgIn_5S_8$ film electrodes prepared by chemical bath deposition

Kong-Wei Cheng[a,b,*], Chao-Ming Huang[c], Guan-Ting Pan[d], Jau-Chyn Huang[e], Tai-Chou Lee[f], Thomas C.K. Yang[d]

[a] Department of Chemical and Materials Engineering, Chang Gung University, Taoyuan, Taiwan
[b] Solar Cell Group, Green Technology Research Center, Chang Gung University, Taoyuan, Taiwan
[c] Department of Environmental Engineering, Kun Shan University, Tainan, Taiwan
[d] Department of Chemical Engineering, National Taipei University of Technology, Taipei, Taiwan
[e] Energy and Environmental Laboratory, Industrial Technology Research Institute, Hsinchu, Taiwan
[f] Department of Chemical Engineering, National Chung Cheng University, Chiayi, Taiwan

ARTICLE INFO

Article history:
Received 28 April 2008
Received in revised form 2 October 2008
Accepted 30 November 2008
Available online 11 December 2008

Keywords:
Photoelectrochemical reaction
Optical property
Crystalline
Electrode

ABSTRACT

The Sb-doped $AgIn_5S_8$ films were grown on indium–tin–oxide substrates using chemical bath deposition. The X-ray diffraction patterns of samples show the polycrystalline $AgIn_5S_8$ phase in these films. With the molar ratio of Sb/Ag in the solution higher than 0.2, the conduction type of samples turns into p-type. The thickness, energy band gaps, and carrier densities of these samples are in the range of 692–1119 nm, 1.71–1.73 eV and 5.75×10^{14} to 9.85×10^{14} cm^{-3}, respectively. The maximum photocurrent density of samples with external potential kept at 1.0 V vs. an Ag/AgCl reference electrode was found to be -2.73 mA/cm^2 under illumination using a 300 Xe lamp system.

1. Introduction

Renewable energy has become an important development field due to the increasing demand for fossil fuels and energy in general. To generate storable chemical energy from solar energy is thus an important goal for a clean energy society. One way of achieving this is solar water splitting with a photoelectrochemical (PEC) system. PEC technology has been extensively studied since the Fujishima and Honda effect, which involved a TiO_2 electrode, was reported in 1972 [1]. However, the performance of TiO_2 has been limited to ultraviolet light due to its large band gap, 3.0–3.2 eV. To improve the efficiency of water splitting, various visible light active semiconductors have been developed. Among these new semiconductors, I–III–VI (I = Cu, Ag; III = Al, In, Ga; VI = S, Se, Te) ternary chalcopyrite semiconductors with the general formula I–III–VI_2 have been receiving great interests during the past decade because of their potential applications in PEC devices and solar cells. Tsuji et al. [2–4] proposed the visible light active $AgInS_2$/ZnS, $CuInS_2$/ZnS, and $AgInS_2$/$CuInS_2$/ZnS solid solution photocatalysts with maximum hydrogen evolution rate up to 8.2 L/(h m^2) from an aqueous solution containing sacrificial reagents SO_3^{2-} and S^{2-} under the visible light irradiation. Other types of ternary system I–III–VI semiconductors with the general formula I–III_5–VI_8 are also considered as effective materials in electrical, optical and energy applications [5,6]. Although the photocatalyst in powder form is a simple, cheap process to generate hydrogen by irradiation with sunlight, separation and recycling of the particles have to be employed after use. From the viewpoint of industrial applications, a stable, efficient light absorption and thin film system is more convenient for collecting hydrogen in the photoelectrochemical reaction without further separation procedures. In order to design a new thin film reactor, it is necessary to understand the properties of these new semiconductor films.

Semiconductor films can be prepared by a variety of deposition methods, such as electrodeposition [7], thermal evaporation [8] and solution growth techniques [9,10]. Among these methods, chemical bath deposition (CBD) is an interesting process that has the ability to fabricate low cost, high quality and large area of semiconductor thin films with low consumption of energy. The Ag–In–S ternary semiconductors are the good photo-absorbers for PEC devices because their energy band gaps lie between 1.7 and 1.9 eV [11,12]. However, most of Ag–In–S ternary systems are n-type

* Corresponding author at: Department of Chemical and Materials Engineering, Chang Gung University, No. 259 Wen-Hwa 1st Road, Kwei-Shan, Taoyuan 333, Taiwan, ROC. Tel.: +886 3 2118800x3353; fax: +886 3 2118668.
E-mail address: kwcheng@mail.cgu.edu.tw (K.-W. Cheng).

1010-6030/$ – see front matter.
doi:10.1016/j.jphotochem.2008.11.018

semiconductors. For PEC reactions in electrolytes, p-type semiconductors generally offer some protection against photocorrosion because the surface is cathodically protected under illumination [13]. Yashino et al. [14] prepared the Sb-doped $AgInS_2$ crystals by the hot press method at 400–700 °C for 1 h under high pressure (10 MPa). Their Sb-doped $AgInS_2$ crystals show p-type conductivity. Albor-Aguilera et al. [15] observed p-type conductivity in Sn-doped $AgInS_2$ films using chemical spray pyrolysis. However, there are few reports about the synthesis and characterization of p-type Ag–In–S ternary system semiconductor thin films using solution growth techniques. In this study, the preparation of Sb-doped $AgIn_5S_8$ films on indium–tin–oxide (ITO)-coated glass substrates using chemical bath deposition were developed under aqueous acidic solutions. The structural, optical, and PEC performances of such samples have also been investigated.

2. Experimental

Sb-doped $AgIn_5S_8$ films were grown on ITO-coated glass substrates using chemical bath deposition. Silver nitrate ($AgNO_3$), indium nitrate ($In(NO_3)_3{\cdot}5H_2O$), thioacetamide (CH_3CSNH_2, TAA), and antimony chloride ($SbCl_3$) purchased from Merck. Co. and Sigma–Aldrich Co. with purity better than 99% were the sources of Ag^+, In^{3+}, S^{2-}, and Sb^{3+} ions, respectively. Triethanolamine ($C_6H_{15}NO_3$, TEA) and ammonium nitrate (NH_4NO_3), with the purity better than 99% provided from Merck and Sigma–Aldrich Co. are the complex agent and the buffer, respectively. ITO-coated glass substrates provided from Union Chemical Co. were carefully cleaned ultrasonically in acetone, deionized water, and subsequently ethanol for 30 min each. Finally, the ITO-coated glass substrates were washed carefully using deionized water and blown dry under ultra-pure nitrogen gas.

The Sb-doped $AgIn_5S_8$ films on ITO-coated glass substrates were prepared from a solution bath containing $AgNO_3$, $In(NO_3)_3$, thioacetamide and $SbCl_3$. The same concentration (0.4 M) of solutions for $AgNO_3$ and $In(NO_3)_3$ were mixed in appropriate volumes to obtained the molar ratio of Ag:In as 1:1. 7.4 M triethanolamine solution with appropriate volumes was mixed with the solutions containing Ag^+ and In^{3+} to form the silver and indium complexes. The antimony chloride with appropriate amounts and 0.4 M ammonium nitrate solutions with appropriate volumes were added into the solution containing silver and indium complexes as the source of Sb ions and the buffer, respectively. In order to avoid the formation of hydroxide-complexes such as $In(OH)_3$, the pH value of the solution has to be acidic [16] and sulfuric acid was used to achieve this (solution A). The 0.4 M thioacetamide solution provided S^{2-} ions for the growth of films (solution B). The appropriate amount of thioacetamide solution was added into solution A and mixed well. The final reaction solutions were kept around 20 mL by adding some water into the solution. The detailed reaction parameters are listed in Table 1.

The possible deposition mechanism of Sb-doped $AgIn_5S_8$ ternary semiconductor films are described with the following reactions:

The decomposition of thioacetamide:

$$CH_3CSNH_2 + H^+ \rightarrow H_2S + CH_3CNH^+$$

$$H_2S + H_2O \rightarrow HS^- + H_3O^+$$

$$HS^- + H_2O \rightarrow S^{2-} + H_3O^+$$

The cations react with S^{2-} to form Sb-doped $AgIn_5S_8$ materials:

$$Ag^+ + 5In^{3+} + 8S^{2-} + xSb^{3+} \rightarrow \text{Sb-doped}AgIn_5S_8$$

Due to the low solubility, most Sb-doped $AgIn_5S_8$ materials formed as powders suspended in solution instead of film deposited on ITO-coated glass substrates. To minimize the powders forming, a complexing agent is added into the solution to form complexes with these metal ions. The Sb-doped $AgIn_5S_8$ films can be obtained in an appropriate complexing agent that allows us to control the release rate of Ag^+, In^{3+}, and Sb^{3+} in solution. Without the complexing agent, there is no film grown on the substrates. The most widely used complexing agents are ammonia, triethanolamine, or ethylenediaminetetraacetic acid (EDTA). In this study, triethanolamine was used as the complexing agent for the film deposition. With the addition of triethanolamine, cations of Ag^+ and In^{3+} in solution can be complexes:

$$Ag^+ + TEA \rightarrow Ag(TEA)^+$$

$$In^{3+} + TEA \rightarrow In(TEA)^{3+}$$

The complex and sulfide ions migrate to the substrate surface, where the heterogeneous process takes place to form Sb-doped $AgIn_5S_8$ films:

$$Ag(TEA)^+ + 5In(TEA)^{3+} + 8S^{2-} + xSb^{3+} \rightarrow \text{Sb-doped}AgIn_5S_8(\text{film})$$

Pre-cleaned ITO-coated glass substrates were placed vertically into the reaction solution with the temperature kept at 80 °C. The reaction solution was put on a hot plate with magnetic stirring. Multiple depositions were carried out with a freshly prepared solution bath after a period of 30 min. The total deposition time of 2 h was used in this study. Since the ITO-coated glass substrate was damaged during the high temperature thermal treatment (>550 °C), the temperature of thermal treatment for these films was set at 550 °C. The films prepared in this study were annealed for 1 h in an evacuated quartz tube at 550 °C after final deposition.

The crystallographic study of films was measured using an X-ray diffractometer, Model Rigaku RINT 2000, with Cu Kα (λ = 1.5405 Å) radiation in the 2θ-range from 20° to 70°. The surface morphology and compositions of samples were analyzed using a scanning electron microscope equipped with energy dispersive analysis of X-ray (EDAX), Model JEOL JSAM 6700F. The accelerating voltage of

Table 1
The deposition parameters of Sb-doped $AgIn_5S_8$ samples prepared in this study.

Samples	Solution A						Solution B	Mixture of solutions A and B
	0.4 M $AgNO_3$ (mL)	0.4 M $In(NO_3)_3$ (mL)	0.4 M NH_4NO_3 (mL)	$SbCl_3$ (g)	7.4 M TEA (mL)	18 M H_2SO_4 (mL)	0.4 M TAA (mL)	Mole ratios of Ag/In/S/Sb
(a)	1.10	1.10	0.55	0.00	0.55	1.43	15.6	1:1:14:0.0
(b)	1.11	1.11	0.55	0.01	0.55	1.11	15.5	1:1:14:0.1
(c)	1.10	1.10	0.55	0.02	0.55	1.10	15.4	1:1:14:0.2
(d)	1.09	1.09	0.55	0.03	0.55	1.10	15.3	1:1:14:0.3
(e)	1.09	1.09	0.54	0.04	0.54	1.09	15.2	1:1:14:0.4
(f)	1.08	1.08	0.54	0.05	0.54	1.08	15.1	1:1:14:0.5

SEM was set at 10 kV. The spectral transmittances of the films were measured by the normal incident double beam UV–vis–NIR spectrophotometer (Perkin-Elmer Lambda 900) in the wavelength range from 300 to 2000 nm at room temperature with air as the reference. The absorptions of films were also measured by placing an identical ITO-coated glass substrate as the reference. The optical properties of samples in this study were obtained using transmittance spectra and data regression.

The Mott–Schottky plots of the samples were measured using a computer-controlled potentiostat (Autolab Model PGSTAT 30) equipped with a frequency response analyzer (Autolab FRA2 modules). The measurements were carried out under the following conditions: the electrolyte solutions of 0.5 M K_2SO_4 with pH values at 6, 8, and 10. The applied potentials were in the range of −1.0 to +1.0 V vs. an Ag/AgCl reference electrode. For the frequencies higher than 1 kHz, the equivalent circuit can be simplified into a series of resistance–capacitance (RC) circuits. In this study, the frequency of impendence measurement was set at 1 kHz to obtain the Mott–Schottky plots for the samples.

The PEC performances of these samples were carried out in a Pyrex electrolytic cell. The sample, a Pt plate electrode (both with an average area of 1.0 cm^2), and an Ag/AgCl electrode were employed as working, counter and reference electrodes, respectively. A Cu wire was attached to the conducting layer of a working electrode with silver paste, and the back contact and edges of the working electrode were sealed with epoxy resin. The aqueous K_2SO_3 (0.25 M) and Na_2S (0.35 M) solution, prepared using double deionized water and degassed by purging with Argon gas (99.99% purity) before each experiment, was used as the electrolyte. The electrolytes were then put into an ultrasonic bath for 30 min before each experiment in order to decrease the influence of gas solutes. Photocurrent measurements, as a function of applied potential, were carried out using a computer-controlled potentiostat (Autolab Model PGSTAT 30) for all PEC experiments, both in the dark and under illumination. The sweep rate of applied potential was set at 5 mV/s. A 300 W Xe short arc lamp (Perkin-Elmer Model PE300BF) with light intensity kept at 100 mW/cm^2 was employed to simulate solar light. The quantum efficiency under monochromatic light illumination was measured using a monochromator (Sciencetech Model 9030) assisted by an automatic filter wheel placed between the photoelectrochemical cell and the light source.

3. Results and discussion

3.1. Crystal structure analysis

Fig. 1 shows the X-ray diffraction patterns of Sb-doped $AgIn_5S_8$ films prepared under various Sb-doped ratios using chemical bath deposition. The standard diffraction peaks of $AgIn_5S_8$ [17] reported in JCPDS cards are also shown in Fig. 1. Only the cubic polycrystalline $AgIn_5S_8$ phase is observed. The X-ray diffraction patterns of samples indicate no Sb alloy or other binary or ternary compounds including Sb atoms were present in these samples. The intensities of the cubic $AgIn_5S_8$ phase decrease with an increase in the molar ratio of Sb in the reaction solution. This is because there are some intrinsic defects in the crystal structure as Sb-doped is increased, which effectively decrease the crystalline of the film. A small shift in the peaks to a higher angle with an increase in Sb content in the film is observed in Fig. 1. The lattice constants of samples estimated using XRD diffraction patterns are in the range of 1.083–1.080 nm, which decrease with an increase in molar ratio of Sb in the reaction solution. Fig. 2 shows the effects of Sb ions in the reaction solution on the lattice constants of samples in this study. These results are reasonable because the ion radii of S^{2-} (1.84 Å) are larger than Ag^+(1.14 Å), In^{3+}(0.76 Å) and Sb^{3+} (1.40 Å) [4,18,19]. Yoshino et al.

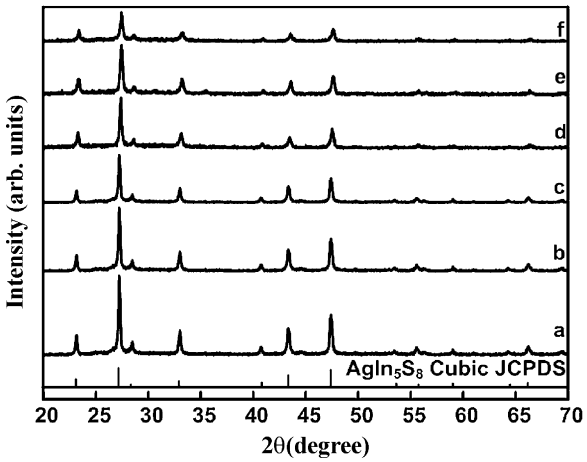

Fig. 1. X-ray diffraction patterns of samples deposited on ITO-coated glass substrates under various deposition parameters using chemical bath deposition.

[14] shows that the Sb atoms can occupy the S sites in the Sb-doped $AgInS_2$ film. The shift can thus be explained by the small difference in Sb and S atomic radii.

3.2. Optical properties

The transmittance spectra of semiconductor films obtained by chemical bath deposition are shown in Fig. 3. The transmittance spectra of samples prepared in this study show oscillatory behaviors in the wavelength range from 1000 to 2000 nm. This is because the interference pattern between the wave fronts is reflected from the two surfaces of the film. The refractive index, extinction index, energy gap, and thickness of the film grown on substrate are the important properties for the design of a PEC cell. Thickness and optical constants can be obtained from transmittance spectra with data regression. Some formulas for the various transmittance spectra of the film on transparent substrates have been proposed [20–22]. The transmittance spectra of films grown on ITO-coated glass substrates were fitted using the following formula [22]:

$$T = \frac{64 n_0^2 n_s^2 (n^2 + k^2)}{a_1 \exp(b) + a_2 \exp(-b)} \quad (1)$$

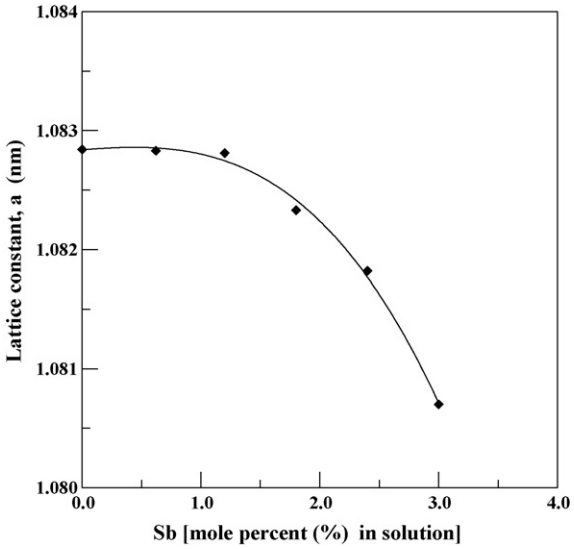

Fig. 2. Effect of Sb on the lattice constants of samples in this study.

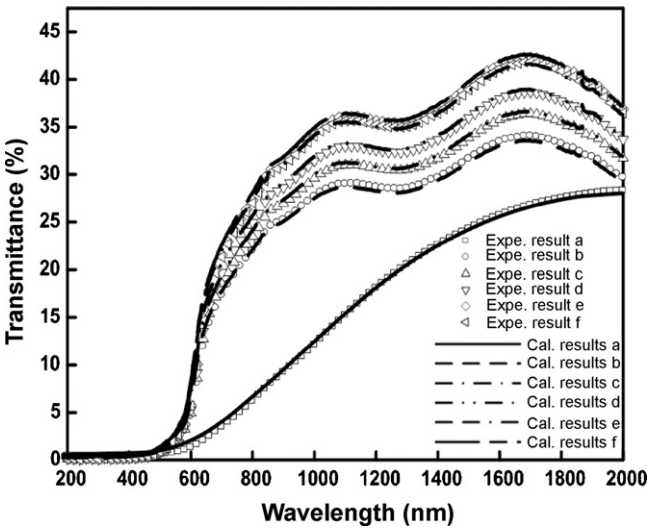

Fig. 3. Transmittance spectra of the samples prepared in this study.

$$a_1 = 2\{(n_0+n)^2+k^2\}\{(n_s^2+n_0^2)(n_s^2+n^2+k^2)+(4nn_0n_s^2)\} \quad (2)$$

$$a_2 = 2\{(n_0-n)^2+k^2\}\{(n_s^2+n_0^2)(n_s^2+n^2+k^2)-(4nn_0n_s^2)\} \quad (3)$$

$$b = \frac{4\pi kd}{\lambda} = \alpha d \quad (4)$$

where n, k, α and d are the refractive index, extinction coefficient, absorption coefficient and thickness of film, respectively. n_0 and n_s are the refractive indices of air (refractive index = 1) and the substrate.

Various dispersion equations for $n(\lambda)$ and $k(\lambda)$ have been proposed to described the optical properties of the films. The dispersion equations for n and k that satisfy Kramers–Kronig relation were proposed by Forouhi and Bloomer [23]. The Forouhi dispersion equations are:

$$n(E) = n(\infty) + \sum_{i=1}^{q}\left[\frac{(B_{0,i}E + C_{0,i})}{(E^2 - B_iE + C_i)}\right] \quad (5)$$

$$k(E) = \sum_{i=1}^{q}\left\{\frac{[A_i(E-E_g)^2]}{(E^2 - B_iE + C_i)}\right\} \quad \text{for } E > E_g, \quad k(E) = 0 \quad \text{for } E < E_g \quad (6)$$

where E is the incident photon energy, E_g is the optical energy bandgap of film, A, B, C and $n(\infty)$ are the independent parameters. B_0, C_0 are related to the independent parameters as follows:

$$B_{o,i} = \frac{A_i}{Q_i}\left(-\frac{B_i^2}{2} + E_gB_i - E_g^2 + C_i\right) \quad (7)$$

$$C_{0,i} = \frac{A_i}{Q_i}\left[(E_g^2 + C_i\left(\frac{Bi}{2}\right) - 2E_gC_i\right] \quad (8)$$

$$Q_i = \frac{1}{2}(4C_i - B_i^2)^{1/2} \quad (9)$$

where $4C_i - B_i^2 > 0$. In this study, it is assumed that it is possible to fit the experimental transmittance data by using one term ($q = 1$) of the Forouhi and Bloomer equation. The refractive index of substrate n_s was obtained by fitting the transmittance spectrum of the ITO-coated glass substrate. The dispersion equation of Forouhi and Bloomer functions was employed in this study. The refractive index n, extinction coefficient k, and thickness of film d can be obtained by fitting the experimental transmittance spectra with the iterative method. Table 2 shows the values of the Forouhi and Bloomer dispersion equation parameters obtained from the transmittance spectra and absolute average deviations (AAD) of transmittance spectra for Sb-doped $AgIn_5S_8$ films on ITO-coated glass substrates. Fig. 3 shows the results calculated using the Forouhi and Bloomer dispersion equation and formula of transmittance spectrum for Eq. (1). The calculated results agreed well with experimental data for these films. The thicknesses of films with various Sb contents obtained from Forouhi and Bloomer dispersion equation are listed in Table 2. The thicknesses of the films deposited on ITO-coated glass substrates are in the range of 692–1114 nm. The thickness of films decreases with an increase in molar ratio of Sb in solution. Figs. 4 and 5 show the relations between refractive index n, extinction coefficient k, and wavelength using the Forouhi and Bloomer dispersion equation and formula of transmittance spectrum in Eq. (1), respectively. Both refractive index and extinction coefficient decrease with increasing wavelength of the incident light and approach zero when the incident light wavelength greater than 800 nm. There are some reports that have been published about the band gap of $AgIn_5S_8$ films. Their results show the band gap of $AgIn_5S_8$ film is in the range of 1.7–1.8 eV [24,25]. The optical properties of samples agree well with the XRD results. Fig. 6 shows the UV–vis–NIR absorption spectra for samples prepared in this study. The spectrum of sample (a) shows the absorption edge at 730 nm and a little absorption shifted towards the shorter wavelength side with an increase in the molar ratio of Sb in reaction solutions. Deshmukh et al. [26] shows the Sb doping in CdS generates charge-trapping centers in the band gap which effectively decrease the crystallinity, and therefore an increase in the band gap of CdS is observed. The absorption edge of sample (f) approached

Table 2
Calculated results of transmittance spectra for Sb-doped $AgIn_5S_8$ samples using Forouhi–Bloomer dispersion equation.

Samples	Forouhi–Bloomer dispersion equation						
	A	B (eV)	C (eV^2)	$n(\infty)$	E_g (eV)	d (nm)	AAD (%)[a]
(a)	6.92	2.05	0.08	0.73	1.71	1119	1.71
(b)	6.62	1.98	0.14	0.79	1.72	913	2.38
(c)	6.57	1.93	0.16	0.87	1.72	806	2.03
(d)	6.52	1.91	0.19	0.92	1.73	729	1.95
(e)	6.41	1.88	0.24	1.07	1.73	717	1.87
(f)	6.39	1.87	0.27	1.21	1.73	692	1.77

[a] AAD (%) $= \frac{100}{L}\sum_{i=1}^{L}|T_{cal,i} - T_{exp,i}|/T_{exp,i}$, L is the number of transmittance spectra data.

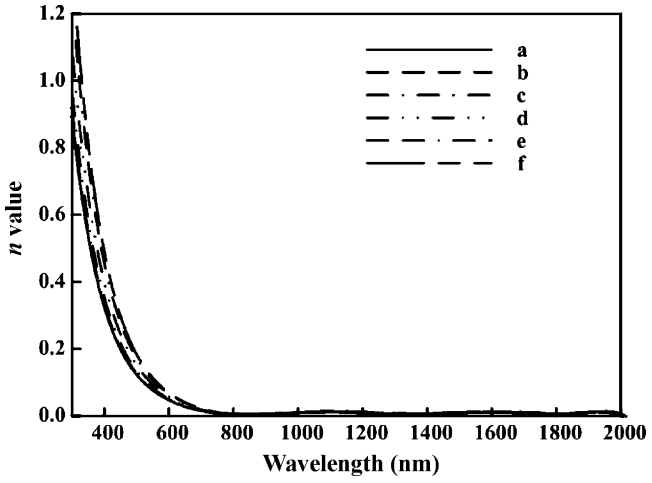

Fig. 4. The relations between refractive index n and wavelength of incident light for Sb-doped $AgIn_5S_8$ polycrystalline films in this study.

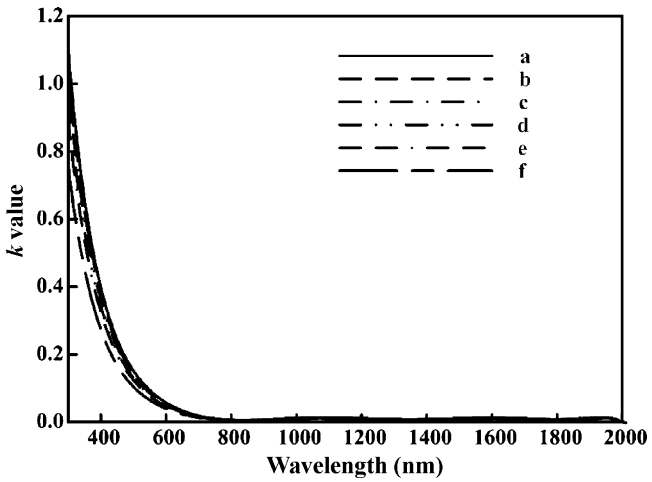

Fig. 5. The relations between extinction coefficient k and wavelength of incident light for Sb-doped $AgIn_5S_8$ polycrystalline films in this study.

710 nm, which agreed with the results obtained from the Forouhi and Bloomer dispersion equation and results from Deshmukh et al. [26].

3.3. Microstructure and compositions studies

Fig. 7 shows the SEM images of samples (a), (d) and (f) at 40 K (X). The SEM images show that the microstructures of the surface change with an increase in the Sb content of the films. Diamond-like microstructures are observed on the surface of sample (a). Plate-like microstructures are observed for the surfaces of samples (d) and (f).

Quantitative analysis using energy dispersion X-ray analysis (EDAX) was employed in this study to analyze the atomic ratios of Ag, In, S, and Sb in samples prepared in this study. The atomic ratios of elements for these samples are shown in Table 3. The atomic ratios of [Ag]:[In]:[S]:[Sb] of samples from EDAX analysis are in the range of 1:3.08–4.94:6.77–6.35:0–0.04. In our pervious work, the results show some low crystalline $AgInS_2$ phase form in the film, and make the atomic ratios of [Ag]:[In]:[S] of samples in the range of 1:1:2–1:5:8 [27]. It is observed that the ratios of In/Ag and Sb/Ag of the films increase with an increase in molar ratio of Sb in the reaction solution. The ratio of S/Ag in the film decreases with an increase in molar ratio of Sb in reaction solution. The Sb-doped

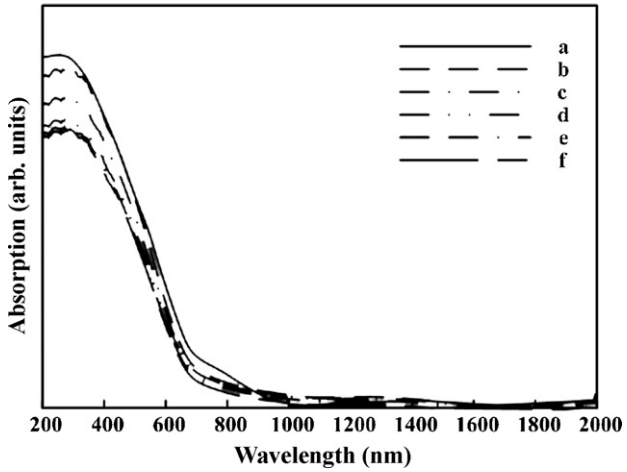

Fig. 6. UV–vis–NIR absorption spectra of samples prepared in this study.

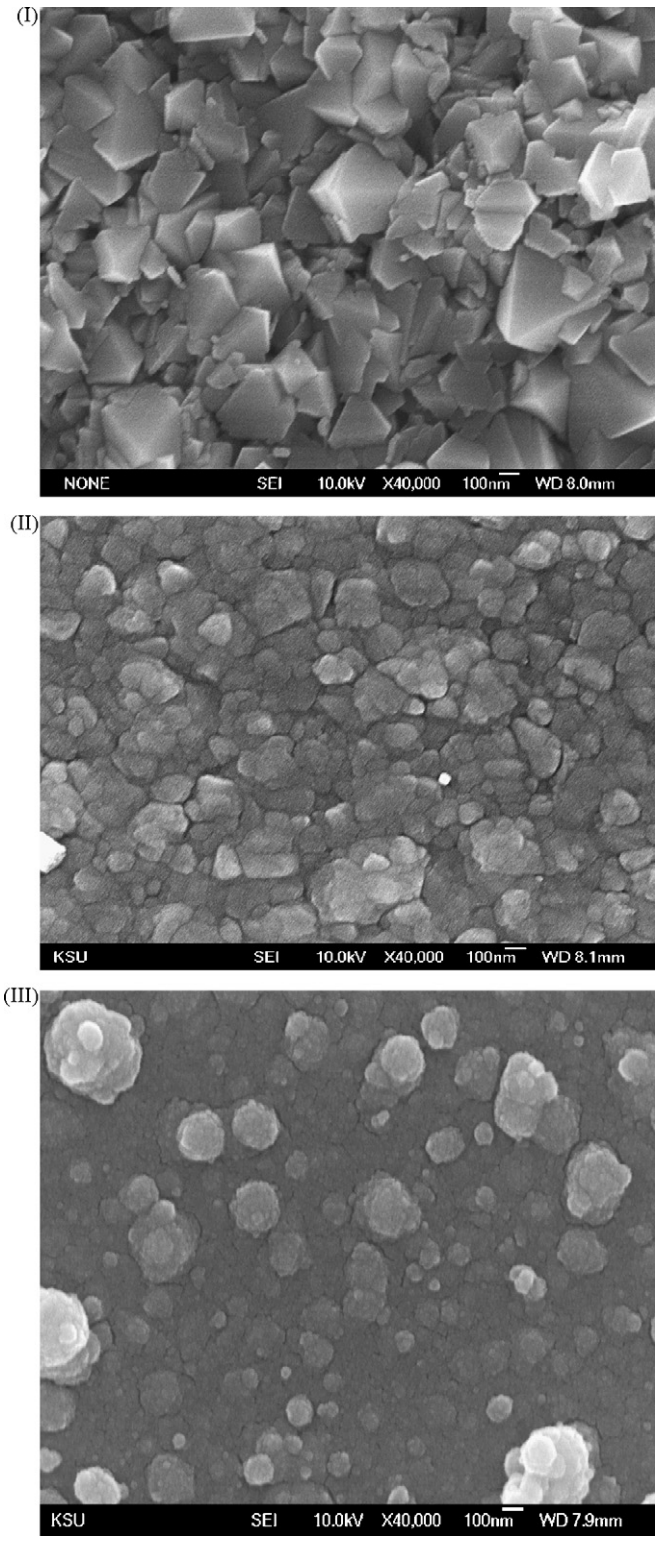

Fig. 7. The SEM images of films prepared in this study: (I) sample (a), (II) sample (d), and (III) sample (f).

$AgIn_5S_8$ films (samples (b)–(f)) prepared in this study become S-poor with an increase in Sb doping concentrations compared with the un-doped sample (sample (a)), which indicate that the Sb atom can occupy the S site, and some S vacancies in the films are also presented. These results agree well with the XRD diffraction patterns and the results of Yashino et al. [14].

Table 3
The molar ratios of elements for Sb-doped $AgIn_5S_8$ films using chemical bath deposition.

Samples	Atomic percents (%)				Molar ratios of element for films			
	Ag	In	S	Sb	Ag	In	S	Sb
(a)	9.21	28.40	62.38	–	1.00	3.08	6.77	–
(b)	8.43	35.26	56.24	0.07	1.00	4.18	6.67	0.008
(c)	8.32	37.46	54.11	0.11	1.00	4.50	6.50	0.013
(d)	8.21	38.89	52.77	0.13	1.00	4.74	6.43	0.016
(e)	8.14	39.43	52.21	0.22	1.00	4.84	6.41	0.027
(f)	8.11	40.04	51.51	0.34	1.00	4.94	6.35	0.042

3.4. Electrical properties

Study of the semiconductor/electrolyte Schottky barrier is important in solar energy and rectification applications. Several methods for studying the Schottky barrier have been proposed. One method based on the capacitance vs. applied potential measurement is the Mott–Schottky relationship for the barrier. The Mott–Schottky equation is given as follows:

$$\frac{1}{C^2} = B \times \left[\frac{2}{\varepsilon\varepsilon_0 e N_D A^2}\right]\left[E - E_{FB} - \left(\frac{kT}{e}\right)\right] \quad (10)$$

where ε is the dielectric constant of the semiconductor, A is the surface area of the interface, N_D is the carrier density of the semiconductor, E_{FB} is the flat band potential of the semiconductor, which is close to the potential of Fermi level for the semiconductor, e is the electronic charge, and ε_0 is the permittivity of the vacuum. For an n-type semiconductor, B is equal to 1, while for a p-type semiconductor, B is equal to −1. From this relationship, E_{FB} can be obtained from E_0, the point of intersection of a C^{-2} vs. E plot with the E-axis:

$$E_0 = E_{FB} + \frac{kT}{e} \quad (11)$$

If, furthermore, ε and A are known, N_D can be determined. Fig. 8 shows the Mott–Schottky plots for the different samples in this study. It is observed that C^{-2} vs. applied potential E produces three straight lines; moreover, the relationship between C^{-2} and E is almost independent of the pH values of the electrolyte solution. It is known that sulfur species semiconductors do not react with H^+ or OH^- ion in solution. The band edges at the interface do not shift with the pH values of the solution. Table 4 shows the values of flat band potentials of samples prepared in this study. The flat band potentials of these samples lie in the range of −0.403 to +0.127 V vs. normal hydrogen electrode (NHE) (−0.61 to −0.08 V vs. an Ag/AgCl electrode) for n-type, while 0.477–0.787 V vs. (NHE) (0.27–0.58 V vs. an Ag/AgCl electrode) for p-type, which become more positive with the increase of molar ratios of Sb in reaction solution. The values of carrier density of samples obtained from the Mott–Schottky plots are also presented in Table 4. The carrier densities of Sb-doped $AgIn_5S_8$ films obtained from the Mott–Schottky plots are in the range of 5.75×10^{14} to 9.85×10^{14} cm^{-3}, which increase with an increase in molar ratio of Sb. The conduction types

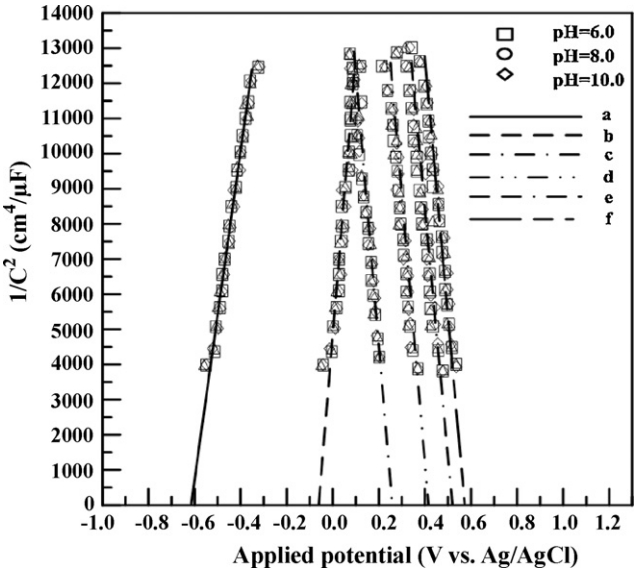

Fig. 8. Mott–Schottky plots of the samples under various deposition parameters in this study.

of samples (a) and (b) grown from chemical bath deposition are the n-type semiconductors, while samples (c)–(f) are the p-type semiconductors. The positions of conduction band and valance band for semiconductor can be obtained from flat band potentials and some physical properties such as the carrier effective mass and acceptor or donor impurity concentration for semiconductor. The carrier effective mass of $AgIn_5S_8$ is 0.2 m_0 [28], where m_0 is the mass of electron. The positions of the valance band and conduction band for the samples determined by the transmittance spectra and electrochemical analysis in this study are shown in Table 4.

The PEC performances of samples were carried out to examine the possibility of solar energy applications. Fig. 9 shows the photocurrent densities of the n-type $AgIn_5S_8$ films prepared in this work with the applied potentials in the range between −1.0 and 1.0 V vs. an Ag/AgCl electrode. It is observed that the photocurrent densities of samples (a) and (b) reached to 0.68 and 0.19 mA/cm^2 at the external potential +1.0 V vs. an Ag/AgCl electrode, respectively. The fact that the photocurrent occurs on the positive potential area indicates that the films prepared are n-type, which can also be seen from the results of Mott–Schottky plots. The photocurrent density of n-type $AgIn_5S_8$ decreases with an increase in molar ratios of Sb in the reaction solution. The reason is because the flat band potential of sample (b) is more positive than sample (a), the energy potential of electrons for sample (b) is lower than that of sample (a) with the same external bias. The driving force in PEC reaction using sample (b) is smaller than the sample (a) with the same external bias, and the photocurrent density of sample (b) is smaller than the sample (a). Fig. 10 shows the photocurrent densities of the p-type $AgIn_5S_8$ films prepared in this work with the applied potentials in

Table 4
The physical properties of Sb-doped $AgIn_5S_8$ films on ITO-coated glass substrates using chemical bath depositions.

Samples	Carrier density (cm^{-3})[a]	$E_{F_B}^{NHE}$ (V)[a]	$E_{F_B}^{NHE}$ (V)[b]	E_{VB}^{NHE} (V)	E_{CB}^{NHE} (V)	J_{Max} (mA/cm^2)[c]	Conduction type[a]
(a)	5.75×10^{14}	−0.403	−0.40	1.09	−0.62	0.68	n
(b)	5.92×10^{14}	0.127	0.13	1.63	−0.09	0.19	n
(c)	6.37×10^{14}	0.477	0.48	0.69	−1.03	−1.33	p
(d)	6.87×10^{14}	0.627	0.63	0.84	−0.88	−1.91	p
(e)	7.98×10^{14}	0.727	0.73	0.94	−0.79	−2.08	p
(f)	9.85×10^{14}	0.787	0.79	1.00	−0.73	−2.73	p

[a] Calculated from Mott–Schottky plots.
[b] Determined from photocurrent density–applied voltage plots.
[c] Photocurrent density under an illumination intensity of 100 mW/cm^2 and external bias kept at 1.0 V vs. an Ag/AgCl reference electrode.

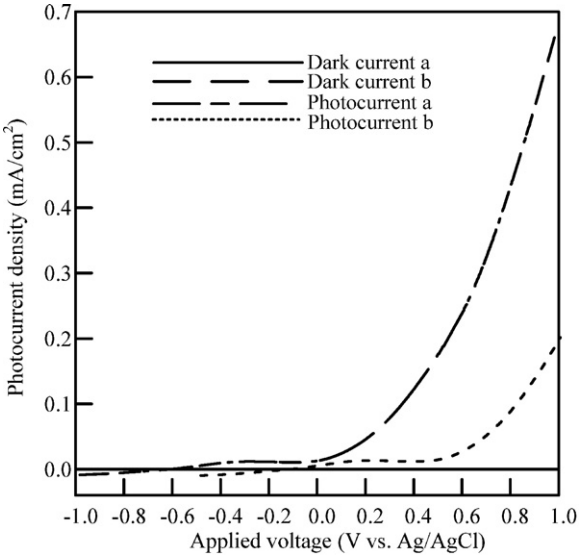

Fig. 9. Photocurrent density–applied voltage plot in the range from −1 to ∼+1 V vs. an Ag/AgCl electrode for n-type $AgIn_5S_8$ films at K_2SO_3 (0.25 M) + Na_2S (0.35 M) aqueous solution.

the range between −1.0 and +1.0 V vs. an Ag/AgCl electrode. It is observed that the photocurrent densities of p-type $AgIn_5S_8$ films in the range of −1.33 to −2.73 mA/cm^2 at the external potential −1.0 V vs. an Ag/AgCl electrode. All of these samples have the photo-enhancement effect. The fact that the photocurrent occurs on the negative potential area indicates that the films prepared are p-type, which can also be seen from the results of Mott–Schottky plots. The photocurrent density of p-type $AgIn_5S_8$ increases with an increase in molar ratios of Sb in reaction solution. Since the flat band potential of sample (f) is more positive than the other p-type samples, the energy potential of holes for sample (f) is the lowest than the other samples with the same external bias. The driving force of sample (f) in PEC reaction is the maximum in all p-type samples in this study. The largest photocurrent density of sample (f) was observed on the same external negative potential. The flat band potentials of samples can be also determined from photocurrent density measurements. The onset of photocurrent density can be treated as a

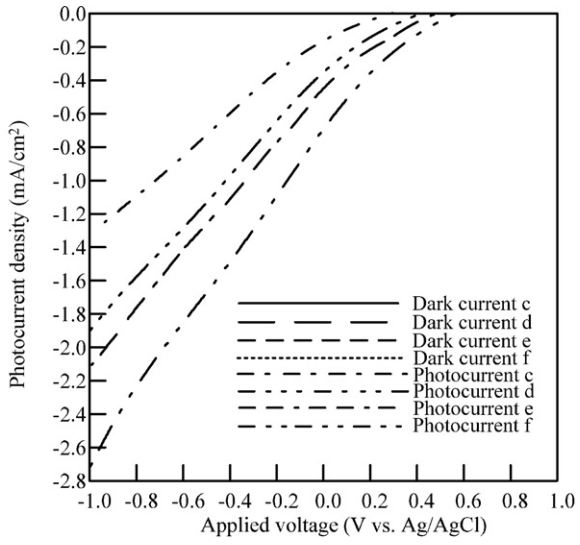

Fig. 10. Photocurrent density–applied voltage plot in the range from −1 to ∼+1 V vs. an Ag/AgCl electrode for p-type $AgIn_5S_8$ films at K_2SO_3 (0.25 M) + Na_2S (0.35 M) aqueous solution.

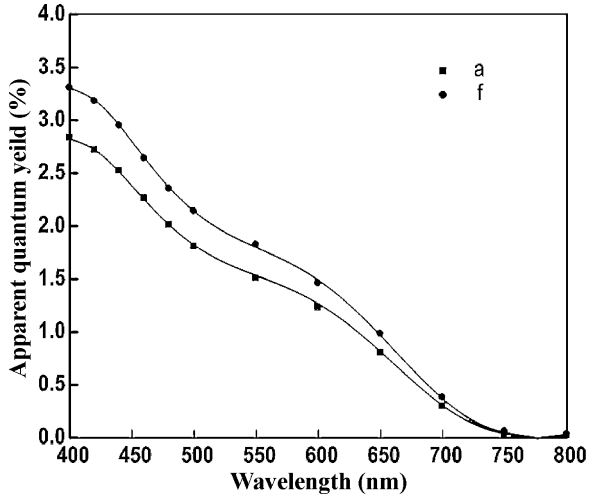

Fig. 11. Plot of quantum efficiency vs. wavelength of incident light for samples (a) and (f) at K_2SO_3 (0.25 M) + Na_2S (0.35 M) aqueous solution with the external bias kept at 1 V.

measure of the flat band potentials, E_{FB} [29,30]. Table 4 shows the flat band potentials of samples obtained from photocurrent density measurements. The values of flat band potentials determined from Mott–Schottky plots and photocurrent density measurements are almost in the same values. The flat band potentials of these samples lie in the range of −0.40 to 0.13 V vs. normal hydrogen electrode for n-type, while 0.48–0.79 V vs. (NHE) for p-type. These experimental results show the samples prepared in this study can be used as absorbers in the PEC application in the solutions.

The calculation of quantum efficiency under monochromatic light illumination, $\eta(\lambda)$, can be carried out using the following equation [31]:

$$\eta(\lambda) = \frac{j_p(\lambda)}{eI(\lambda)} \quad (12)$$

where $j_p(\lambda)$ is the monochromatic photocurrent density (in mA/cm^2), e is the electronic charge, $I(\lambda)$ is the flux of incident photons at wavelength λ, and λ is the wavelength (in nm), respectively.

A two-electrode system with working and counter electrodes was employed for determination of the quantum efficiency of samples (a) and (f) prepared in this study. The K_2SO_3 (0.25 M) + Na_2S (0.35 M) aqueous solution was used as the electrolyte. Fig. 11 shows the quantum efficiency vs. wavelength for samples (a) and (f), ranging from 400 to 800 nm. The quantum efficiency of samples (a) and (f) were found out to be 2.8% and 3.3% respectively, with the wavelength of incident light at 400 nm and the external bias set to 1 V. The onset of the photoelectrochemical response of samples (a) and (f) located around 750 nm, corresponding to band-gaps around 1.65 eV, which is closely consistent with the value of band-gaps presented in Table 2 and the absorption spectra of samples shown in Fig. 6.

4. Conclusions

In this study, the Sb-doped $AgIn_5S_8$ films were deposited on ITO-coated glass substrates using chemical bath deposition and the structural, electric and optical properties of the films were investigated. The XRD patterns show $AgIn_5S_8$ is the major crystalline phase of the films on ITO-coated glass substrates with an increase in molar ratio of Sb. With the molar ratio of Sb/Ag in the solution higher than 0.2, the conduction type of the samples becomes into p-type semiconductor. The band gaps and carrier densities of these samples are in the range of 1.71–1.73 eV, and 5.75×10^{14} to 9.85×10^{14} cm^{-3}, respectively. The flat band potentials of these samples lie in the

range of −0.40 to 0.13 V vs. normal hydrogen electrode for n-type, while 0.477–0.787 V vs. (NHE) for p-type. The maximum photocurrent density of samples prepared in this study was found to be $-2.73\,mA/cm^2$ under the illumination using a 300 Xe lamp system with light intensity set at $100\,mW/cm^2$. From these results, it is found that Sb-doped $AgIn_5S_8$ film deposition on ITO-coated glass using chemical bath deposition is a suitable process for the industrial applications such as the absorbers in PEC.

Acknowledgements

The authors are grateful to the National Science Council (Grant Nos. NSC 95-2218-E-182-003-MY2, NSC-96-ET-7-194-002-ET) and Bureau of Energy, Ministry of Economic Affairs (Grant No. 6455DC5210) for their support for this study.

References

[1] A. Fujishima, K. Honda, Nature 238 (1972) 37–38.
[2] I. Tsuji, H. Kato, A. Kudo, Angew. Chem. Int. Ed. 44 (2005) 3565–3568.
[3] I. Tsuji, H. Kato, H. Kobayashi, A. Kudo, J. Phys. Chem. B 109 (2005) 7323–7329.
[4] I. Tsuji, H. Kato, H. Kobayashi, A. Kudo, J. Am. Chem. Soc. 126 (2004) 13406–13413.
[5] I. Konovalor, O. Tober, M. Winkler, K. Otte, Sol. Energy Mater. Sol. Cells 67 (2001) 49–58.
[6] I. Konovalov, L. Makhova, R. Hesse, R. Szargan, Thin Solid Films 493 (2005) 282–287.
[7] J.L. Orts, R. Diaz, P. Herrasti, F. Rueda, E. Fatas, Sol. Energy Mater. Sol. Cells 91 (2007) 621–628.
[8] I.V. Bodnar, V.F. Gremenok, Thin Sold Films 487 (2005) 31–34.
[9] S.B. Ambade, R.S. Mane, S.S. Kale, S.H. Sonawane, A.V. Shaikh, S.H. Han, Appl. Surf. Sci. 253 (2006) 2123–2126.
[10] A.M. Salem, M.O. Abou-Helal, Mater. Chem. Phys. 80 (2003) 740–745.
[11] L. Makhova, R. Szargan, I. Konovalov, Thin Solid Films 472 (2005) 157–164.
[12] Y. Akaki, S. Kurihara, M. Shirahama, K. Tsurugida, S. Seto, T. Kakeno, K. Yoshino, J. Phys. Chem. Solids 66 (2005) 1858–1861.
[13] O. Khaselev, J.A. Turner, Science 280 (1998) 425–427.
[14] K. Yashino, H. Komaki, T. Kakeno, Y. Akaki, T. Ikari, J. Phys. Chem. Solids 64 (2003) 1839–1842.
[15] M.L. Albor-Aguilera, J.J. Cayente-Romero, J.M. Peza-Tapia, L.R. De Leon-Gutierrez, M. Ortega-Lopez, Thin Solid Films 490 (2005) 168–172.
[16] B. Asenjo, A.M. Chaparro, M.T. Gutierrez, J. Herrero, C. Maffiotte, Electrochim. Acta 49 (2004) 737–744.
[17] JCPDS No. 25-1329, Powder Diffraction File, Joint Committee on Powder Diffraction Standards, ASTM, Newtown Square, PA, USA, 1999.
[18] S.H. Maron, J.B. Lando, Fundamentals of Physical Chemistry, Macmillan Publishing Co., New York, 1974.
[19] P. Wang, N. Chen, Z. Yin, F. Yang, C. Peng, J. Cryst. Growth 290 (2006) 56–60.
[20] M.G. Krishna, J.S. Piller, A.K. Bhattacharya, Thin Solid Films 357 (1999) 218–222.
[21] R. Swanepoel, J. Phys. E: Sci. Instrum. 16 (1983) 1214–1222.
[22] S. Aglian, D. Mangalaraj, Sa.K. Narayandass, G. Mohan Rao, Physica B 365 (2005) 93–101.
[23] A.R. Forouhi, I. Bloomer, Phys. Rev. 34 (1986) 7018–7025.
[24] L.H. Lin, C.C. Wu, C.H. Lai, T.C. Lee, Chem. Mater. 20 (2008) 4475–4483.
[25] N.S. Orlova, I.V. Bondar, E.A. Kudritskaya, Cryst. Res. Technol. 33 (1998) 37–42.
[26] L.P. Deshmukh, S.G. Holikatti, B.M. More, Mater. Chem. Phys. 39 (1995) 278–283.
[27] K.W. Cheng, C.M. Huang, G.T. Pan, W.S. Chang, T.C. Lee, T.C.K. Yang, J. Photochem. Photobiol A: Chem. 190 (2007) 77–87.
[28] A.F. Qasrawi, N.M. Gasanly, Cryst. Res. Technol. 36 (2001) 457–464.
[29] S. Cattarin, P. Guerriero, N. Dietz, H.J. Lewerenz, Electrochim. Acta 40 (1994) 1041–1049.
[30] M. Radecka, M. Rekas, A. Trenczek-Zajac, K. Zakrzewska, J. Power Sources 181 (2008) 46–65.
[31] J. Akikusa, S.U.M. Khan, Int. J. Hydrogen Energy 22 (1997) 875–882.